


Aging exponents for nonequilibrium dynamics following quenches from critical points

Koyel Das, Nalina Vadakkayil, and Subir K. Das*

Theoretical Sciences Unit and School of Advanced Materials, Jawaharlal Nehru Centre for Advanced Scientific Research, Jakkur, Bangalore 560064, India

 (Received 10 February 2020; accepted 20 May 2020; published 4 June 2020)

Via Monte Carlo simulations we study nonequilibrium dynamics in the nearest-neighbor Ising model, following quenches to points inside the ordered region of the phase diagram. With the broad objective of quantifying the nonequilibrium universality classes corresponding to spatially correlated and uncorrelated initial configurations, in this paper we present results for the decay of the order-parameter autocorrelation function for quenches from the critical point. This autocorrelation is an important probe for the aging dynamics in far-from-equilibrium systems and typically exhibits power-law scaling. From the state-of-the-art analysis of the simulation results, we quantify the corresponding exponents (λ) for both conserved and nonconserved (order-parameter) dynamics of the model in space dimension $d = 3$. Via structural analysis we demonstrate that the exponents satisfy a bound. We also revisit the $d = 2$ case to obtain more accurate results. It appears that irrespective of the dimension, λ is approximately the same for both conserved and nonconserved dynamics.

DOI: [10.1103/PhysRevE.101.062112](https://doi.org/10.1103/PhysRevE.101.062112)

I. INTRODUCTION

Following a quench from the high-temperature disordered phase to a point inside the ordered region when a homogeneous system evolves towards the new equilibrium, several quantities [1–7] are of importance for understanding the nonequilibrium dynamics. The structure of a system is usually characterized by the two-point equal time correlation function [1] or by its Fourier transform, S , the structure factor, the latter being directly accessible experimentally. This correlation function, $C(r, t)$, is defined as ($r = |\vec{r}|$)

$$C(r, t) = \langle \psi(\vec{r}, t) \psi(\vec{0}, t) \rangle - \langle \psi(\vec{r}, t) \rangle \langle \psi(\vec{0}, t) \rangle, \quad (1)$$

where $\psi(\vec{r}, t)$ is a space (\vec{r}) and time (t) dependent order parameter. During a “standard” nonequilibrium evolution, $C(r, t)$ exhibits the scaling behavior [1]

$$C(r, t) \equiv \tilde{C}(r/\ell(t)), \quad (2)$$

with ℓ the characteristic length scale, measured as the average size of the domains rich or poor in particles of specific type, typically growing as [1]

$$\ell \sim t^n. \quad (3)$$

While understanding of the scaling form in Eq. (2) and estimation of the growth exponent n in Eq. (3) have been the primary focus [1,2] of studies related to the kinetics of phase transitions, there exist other important aspects as well [5–7]. For example, during the evolution of the ferromagnetic Ising model, the corresponding nearest-neighbor ($\langle ij \rangle$) version of the Hamiltonian being defined as [1]

$$H = -J \sum_{\langle ij \rangle} S_i S_j; S_i = \pm 1; J > 0, \quad (4)$$

one is interested in the time dependence of the fraction of unaffected spins (S_i). This quantity also exhibits a power-law decay with time $t^{-\theta}$, the exponent θ being referred to as the persistence exponent [5]. Furthermore, in an evolving system the time translation invariance is violated, implying different relaxation rates when probed by starting from different waiting times (t_w) or ages of the system. Such an aging property [6–20] is often investigated via the two-time order-parameter autocorrelation function [6]

$$C_{\text{ag}}(t, t_w) = \langle \psi(\vec{r}, t_w) \psi(\vec{r}, t) \rangle - \langle \psi(\vec{r}, t_w) \rangle \langle \psi(\vec{r}, t) \rangle, \quad (5)$$

with $t > t_w$. Despite different decay rates for different t_w , $C_{\text{ag}}(t, t_w)$ in many systems exhibits the scaling property [7]

$$C_{\text{ag}}(t, t_w) \sim (\ell/\ell_w)^{-\lambda}, \quad (6)$$

where ℓ and ℓ_w are the characteristic lengths at t and t_w , respectively.

For the understanding of universality in coarsening dynamics, it is important to study all these properties. Note that universality [1] in nonequilibrium dynamics depends upon the mechanism of transport, space dimension (d), symmetry and conservation of order parameter, etc. In addition, in each of these cases the functional forms or the values of the power-law exponents for the above-mentioned observables may be different for correlated and uncorrelated initial configurations [17,21–26]. In other words, there may be different universality classes depending upon whether a system is quenched to the ordered region with perfectly homogeneous configuration, say, for the Ising model from a starting temperature $T_s = \infty$, with equilibrium correlation length [27] $\xi = 0$, or from the critical point with $\xi = \infty$.

In this work our objective is to estimate λ for initial configurations with $\xi = \infty$ in the three-dimensional Ising model as well as revisit the $d = 2$ case. We consider two cases, viz., kinetics of ordering in uniaxial ferromagnets [1,2]

*das@jncastr.ac.in

and that of phase separation in solid binary ($A + B$) mixtures [1,2]. For the former, the spin values ± 1 in Eq. (4) represent, respectively, the up and down orientations of the atomic magnets. In the second case, different values of S_i stand for an A or a B particle. During ordering in a magnetic system, the volume-integrated order parameter (note that ψ is equivalent to the spin variable) does not remain constant over time [1]. On the other hand, for phase separation in binary mixtures this total value is independent of time [1], i.e., conserved.

Even for such simple models and the technically easier case of $\xi = 0$, estimation of λ remained difficult, particularly for the conserved order-parameter case [9,28]. For quenches from the critical point, additional complexity is expected in computer simulations. In the latter case there exist two sources of finite-size effects [29]. The first one is due to the nonaccessibility of $\xi = \infty$ in the initial correlation [29], and the second is related to the fact [30,31] that $\ell < \infty$, always. Nevertheless, via an appropriate method of analysis [26], in each of the cases we estimate the value of λ quite accurately. It transpires that the obtained numbers are drastically different from those [18] for $\xi = 0$. This is despite the fact that the growth exponent n does not depend upon the choice of initial ξ .

The results are discussed in the background of available analytical information [7,9,17]. It is shown that the numbers obey a bound obtained by Yeung, Rao, and Desai (YRD) [9],

$$\lambda \geq \frac{d + \beta}{2}. \quad (7)$$

Here β is an exponent related to the power-law behavior of the structure factor at the waiting time t_w in the small wave vector (k) limit [32]:

$$S(k, t_w) \sim k^\beta. \quad (8)$$

The rest of the paper is organized as follows. In Sec. II we provide details of the model and methods. Results are presented in Sec. III. Section IV concludes the paper with a brief summary and outlook.

II. MODEL AND METHODS

Monte Carlo (MC) simulations of the nearest-neighbor Ising model [33–35], introduced in the previous section, are performed by employing two different mechanisms, viz., Kawasaki exchange [36] and Glauber spin-flip [37] methods, on a simple cubic or square lattice with periodic boundary conditions in all directions. For this system the value [34] of critical temperature in $d = 3$ is $T_c \simeq 4.51J/k_B$, J and k_B being the interaction strength and the Boltzmann constant, respectively. The corresponding number in $d = 2$ is $\simeq 2.27J/k_B$ [34]. Given that in computer simulations the thermodynamic critical point is not accessible, we have quenched the systems from $T_s = T_c^L$, the finite-size critical temperature for a system of linear dimension L (see the next section for a more detailed discussion on this) [26,29]. The final temperature was set to $T_f = 0.6T_c$, the starting composition always having 50% up and 50% down spins. Below we set J , k_B , and a , the lattice constant that is chosen as the unit of length, to unity.

In the Kawasaki exchange Ising model (KIM), a trial move consists of the interchange of particles between randomly

selected nearest-neighbor sites. For the Glauber Ising model (GIM), a trial move is a flip of an arbitrarily chosen spin. In both the cases we have accepted the trial moves by following the standard Metropolis algorithm [33–35]. KIM and GIM mimic the conserved and nonconserved dynamics, respectively. In our simulations, one Monte Carlo step (MCS), the chosen unit of time, is equivalent to L^d trial moves.

For faster generation of the equilibrium configurations at T_c^L , the Wolff algorithm [38] has been used. There a randomly selected cluster of identical spins/particles has been flipped. This way the critical slowing down [39,40] has been avoided.

The average domain lengths of a system during evolution have been calculated as [31]

$$\ell(t) = \int P(\ell_d, t) \ell_d d\ell_d. \quad (9)$$

Here $P(\ell_d, t)$ is a domain-size distribution function, which is obtained by calculating ℓ_d , the distance between two successive interfaces, by scanning the lattice in all directions. Quantitative results are averaged over a minimum of 100 independent initial configurations for both KIM and GIM. To facilitate extrapolation of the results for aging in the thermodynamically large size limit, we have performed simulations with different system sizes. In $d = 3$ the value of L varies between 24 and 128 for KIM and between 64 and 300 for GIM. In $d = 2$, we have studied systems with L lying in the range [64, 512] for KIM and [64, 1024] for GIM. We have acquired structural data for both types of dynamics for fixed values of L in each of the dimensions. For this purpose, in $d = 3$ we have considered $L = 512$, and the results for $d = 2$ were obtained with $L = 1024$. Given that these system sizes are large we did not simulate multiple values of L in this case. Details on the statistics and the system sizes for the calculations of T_c^L can be found in the next section. Note that most of the results are presented from $d = 3$. We revisit the $d = 2$ case to improve accuracy so that certain conclusions on the dimension dependence can be more safely drawn.

III. RESULTS

As already mentioned, in computer simulations finite-size effects lead to severe difficulties in studies of phenomena associated with phase transitions. In the kinetics of phase transitions, ℓ never reaches ∞ , due to the restriction in the system size [30,31]. This is analogous to the fact that in critical phenomena [29] one always has $\xi < \infty$. Of course, scaling methods exist to overcome the problems in both equilibrium and nonequilibrium contexts [14,18,26,29,30,34,41]. For studies of coarsening phenomena starting from the critical point [23–26], difficulties due to both types of effects are encountered. Nevertheless, via construction of an appropriate extrapolation method [26] we will arrive at quite accurate conclusions.

In critical phenomena the true value of T_c cannot be realized for $L < \infty$. In such a situation, for reaching conclusions in the $L = \infty$ limit, one defines T_c^L , the pseudocritical temperature for a finite system, and relies on appropriate scaling relations [40,42–44]. T_c^L is expected to exhibit the behavior [40,42–45]

$$T_c^L - T_c \sim L^{-1/\nu}, \quad (10)$$

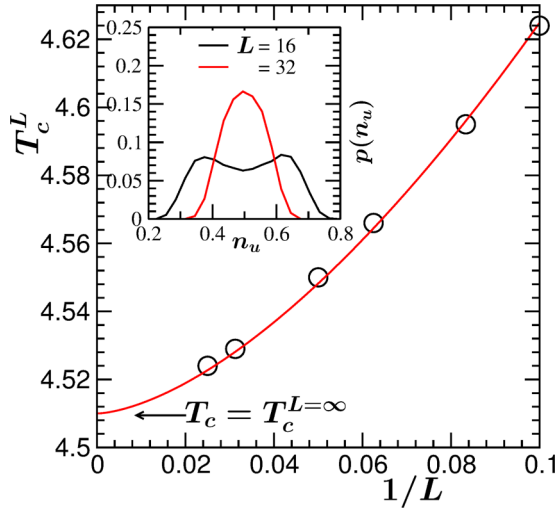


FIG. 1. Finite-size critical temperature T_c^L for the 3D Ising model is plotted as a function of $1/L$. The solid line is a fit to the expected critical behavior [see Eq. (10)] by fixing the correlation length exponent ν to 0.63. The simulation results were obtained via Glauber as well as Wolff algorithms. The arrow points to the value of thermodynamic critical point that also was fixed to the known number. Inset: Order-parameter distributions p for two system sizes, at the same temperature ($T = 4.54$), are plotted vs the concentration (n_u) of up spins.

where ν is the critical exponent corresponding to the divergence [27,45] of ξ at T_c . In Fig. 1 we have presented results for T_c^L , as a function of $1/L$, from $d = 3$. The solid line there is a fit to the scaling form in Eq. (10) by fixing [27,34,45] ν and T_c to the three-dimensional (3D) Ising values ($\simeq 0.63$ and $\simeq 4.51$, respectively). The quality of fit confirms the validity of Eq. (10) as well as the accuracy of the estimations. We use the amplitude ($\simeq 4.4$) obtained from the fit to extract T_c^L for L larger than the presented ones. This number is $\simeq 3.9$ in [26] $d = 2$.

The results in Fig. 1 were obtained by using the Glauber as well as the Wolff algorithms [34,37], exploiting the following facts. The fluctuation in the number of spins or particles of a particular species during simulations provides temperature-dependent probability distributions for the corresponding concentration. These distribution functions are double peaked in the ordered region [26,34]. On the other hand, above criticality one observes single-peak character. The temperature at which the crossover from double- to single-peak shape occurs is taken as the T_c^L for a particular choice of L . In the inset of Fig. 1 we show the distributions, $p(n_u)$ (see caption for the details of the notation), from two different system sizes. For both system sizes the temperature is the same. It is seen that for the larger value of L there is only one peak, while the distribution for the smaller system has two peaks. This is expected in the present setup and is consistent with Eq. (10). Note that the crossover between single-peak and double-peak structures occurs in a continuous manner. Thus, extremely good statistics is needed to identify this. The probability distribution close to T_c^L were thus obtained for each L after averaging over a minimum of 500 independent runs. Only because of this are our results in the main frame of Fig. 1

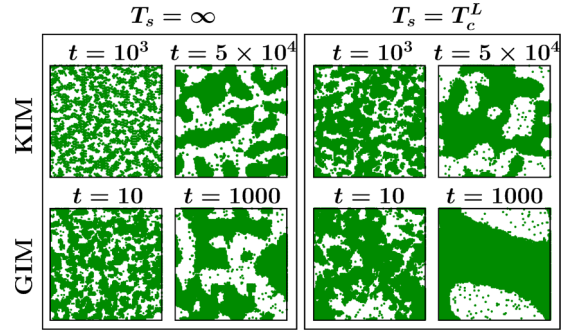


FIG. 2. Two-dimensional sections of the evolution snapshots, recorded during the Monte Carlo simulations of the Ising model in $d = 3$, are presented for quenches to $T_f = 0.6T_c$. The upper frames correspond to conserved dynamics, whereas the lower ones are for the nonconserved case. At the top of each of the frames we have included snapshots for quenches from finite-size critical temperature as well as from $T_s = \infty$, with $L = 128$. In all the frames the down spins (or B particles) are left unmarked.

accurate, the error bars being less than the size of the symbols. T_c^L can also be estimated from the locations of the maxima, with the variation of temperature, in the thermodynamic functions such as susceptibility and specific heat.

To facilitate appropriate analysis of the autocorrelation data, we will perform quenches from T_c^L for different values of L . For each L , the value of λ , referred to as λ_L , will be estimated. Finally, the thermodynamic limit number will be obtained from the convergence of λ_L in the $L = \infty$ limit. In addition to the L dependence, there will be other effects as well. We discuss these in the appropriate places.

In Fig. 2 we present two-dimensional cross sections of the snapshots, taken during the evolution of both types of systems, from $d = 3$. For the sake of completeness we have compared the snapshots for the critical starting temperature with those for quenches with $\xi = 0$, i.e., from $T_s = \infty$. The upper frames are for conserved order-parameter dynamics and the lower ones are for the nonconserved case. In each of the cases the structure for quenches from the critical point appears different from that for $T_s = \infty$. Note that all the presented pictures are from simulations with $L = 128$, and the results for the critical point correspond to quenches from T_c^L , as mentioned above. As is well known [1,31,46–49], it can be appreciated from the figure that in the nonconserved case the growth occurs much faster.

The behavior of the equal time structure factor in $d = 3$ for a thermodynamically large system at criticality is expected to be [27,34,45]

$$S(k, 0) \sim k^{-2}, \quad (11)$$

given that in $d = 3$ the critical exponent η ($\simeq 0.036$, as opposed to 0.25 in $d = 2$), the Fisher exponent that characterizes the power-law factor of the critical correlation as $r^{-(d-2+\eta)}$, has a small value. Typically, in most of the coarsening systems scaling in the decay of autocorrelation function [cf. Eq. (6)] starts from a reasonably large value of t_w . By then the structure is expected to have changed from that at the beginning. Thus, the exponent -2 in Eq. (11) should be verified before being

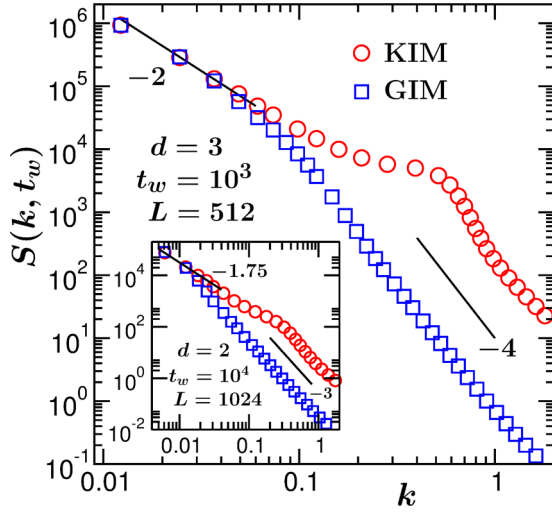


FIG. 3. Log-log plots of structure factor vs wave vector from $d = 3$. Results from both types of dynamics are included. The ordinate of the data set for KIM has been multiplied by a constant number to obtain collapse in the small- k region. Inset: Same as the main frame but for $d = 2$. The solid lines are power laws with exponent values noted in the figure. The values of t_w and L are also mentioned.

taken as the value of β in the YRD bound for understanding of results following quenches from T_c . Furthermore, for $T_s = T_c$, one may even ask about the validity of a stable β . This is related to the question of whether there exists a scaling regime or the structure is continuously changing. Keeping this in mind, in Fig. 3 we present plots of $S(k, t_w)$ versus k for large enough values of L and t_w , from $d = 3$. Results from both dynamics are included. In fact, β appears to be stable at -2 , even though the structural character changes at large k , e.g., an appearance of the Porod law [1] [$S(k) \sim k^{-4}$] is clearly visible that corresponds to the existence of domain boundaries. This value of β , i.e., -2 , will be used later for verifying the YRD bound.

Note here that in Fig. 3 we have presented representative results with appropriate understanding of finite-size effects and onset of scaling in the structure as well as in aging. Even though the results in Fig. 3 are from $L = 512$, simulating this size for long enough time, a necessity in studies of aging phenomena, at $d = 3$ is very time consuming, particularly for the conserved dynamics. So, for aging the presented data are from smaller values of L , and the conclusions in the thermodynamic limit are drawn via appropriate extrapolations.

For the sake of completeness, in the inset of Fig. 3 we present analogous results for $d = 2$. Here also the small k behavior remains unaltered from that in the initial configuration, i.e., we have [27] $\beta = -7/4$. In this dimension the Porod law [1] demands $S(k) \sim k^{-3}$. In the rest of the paper, all figures will contain results for $d = 3$ only, except for the last one.

First results for $C_{ag}(t, t_w)$ are presented in Fig. 4, versus ℓ/ℓ_w , on a log-log scale. In part (a) we have shown data for the nonconserved dynamics, by fixing the system size, for a few different values of t_w . The observations are the following.

There exist sharp departures of the data sets from each other at large ℓ/ℓ_w . The higher the value of t_w , the departure occurs earlier from the plot for a smaller t_w . This is related

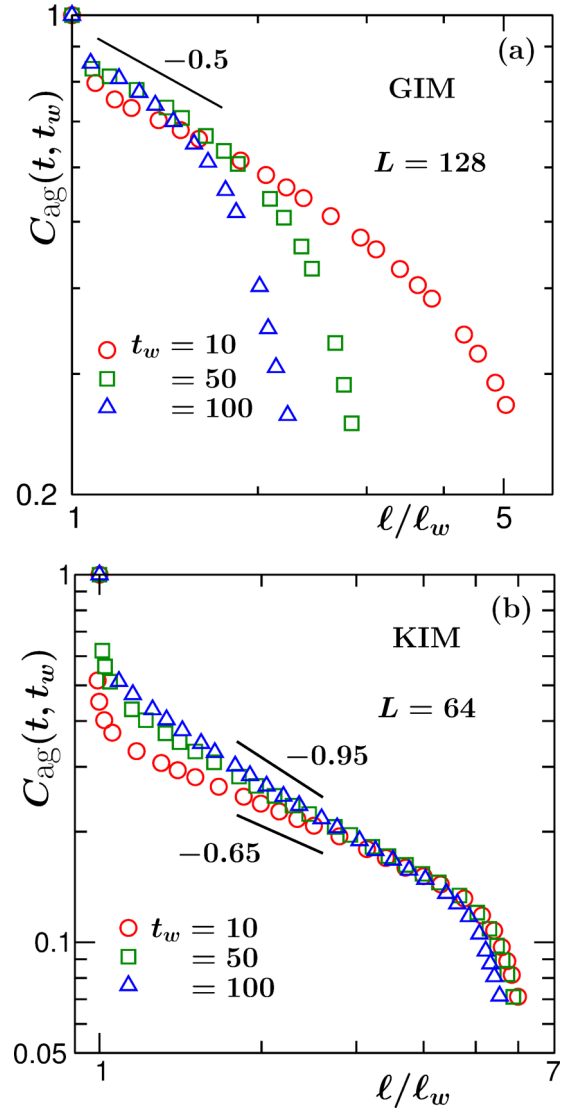


FIG. 4. (a) Log-log plots of the order-parameter autocorrelation function, $C_{ag}(t, t_w)$, vs ℓ/ℓ_w , for the nonconserved dynamics in $d = 3$. Data for a few different values of t_w are included. These results are for $L = 128$. (b) Same as (a) but for the conserved order-parameter dynamics. These results are from simulations with $L = 64$. The solid lines inside both the frames represent power laws, the exponents being mentioned in appropriate places.

to “standard” nonequilibrium finite-size effects [14,18]. With the increase of t_w , a system has less effective size available to grow or age for. This fact can be stated in the following way as well. Note that for a fixed system size the final value of ℓ is fixed. Thus, with the increase of t_w , i.e., of ℓ_w , the value of the scaled variable ℓ/ℓ_w decreases. Naturally, when the latter is chosen as an abscissa variable, the above mentioned departures, with the increase of t_w , start appearing earlier. Furthermore, even in the small ℓ/ℓ_w region the collapse of the data set for $t_w = 10$ with those for the larger t_w values is rather poor. This, we believe, is due to the fact that in the scaling regime the structure is different [32] from the initial configuration [26]. (Also note that the scaling structure for $T_s = T_c$ is different from that for $T_s = \infty$.) During this

switchover to the scaling behavior, the extraction of ℓ is also ambiguous due to continuous change in the structure that thus lacks the property of Eq. (2). If we believe that by $t_w = 50$ the scaling regime has arrived (see the reasonably good collapse of data sets for $t_w = 50$ and 100 in the small ℓ/ℓ_w regime), the corresponding decay is consistent with $\lambda = 0.5$, a value that was predicted theoretically [17]. Nevertheless, given the complexity of finite-size and other effects, further analysis is required before arriving at a conclusion with confidence.

In part (b) of Fig. 4 we present similar results for the conserved dynamics. Here the system size is smaller than in (a). Note that due to slower dynamics in the conserved case ($n = 1/2$ for nonconserved case [1,46], whereas $n = 1/3$ for the conserved dynamics [31,47–49], and these numbers are true irrespective [17,21,50] of T_s), the convergence to the scaling regime has not happened even by $t_w = 100$. For the same reason the onsets of finite-size effects for different t_w values are not so dramatically separated from each other in this case.

For both the dynamics, one gets an impression that the exponent has a tendency to increase with the increase of t_w . The phenomenon of convergence, however, is more complex and requires systematic study involving both t_w and L . This we will perform in the rest of the paper.

Next we examine the effects of system size on the “scaling” regime. We remind the reader that there exists another type of finite-size effect related to $\xi < \infty$. Due to this, with changing system size the exponent will differ in “the scaling regime” as well. Related results are presented in Fig. 5. For the sake of brevity, here we show data only for the conserved case.

In Fig. 5(a) we show $C_{ag}(t, t_w)$ for different values of L versus ℓ/ℓ_w on a log-log scale by fixing t_w to 20. In addition to the delayed appearance of late time finite-size effects, with the increase of system size the decay exponent shows the tendency of shifting towards smaller values [26]. To pick the stable power-law regime appropriately, by discarding the finite size affected and early transient regimes, in Fig. 5(b) we plot the instantaneous exponent [14,18,31,48,49]

$$\lambda_i = -\frac{d \ln C_{ag}(t, t_w)}{d \ln x}; \quad x = \frac{\ell}{\ell_w}, \quad (12)$$

as a function of ℓ/ℓ_w , for two values of L with $t_w = 20$. From the flat parts we extract the L -dependent exponent λ_L . We have performed this exercise for multiple values of t_w for each type of dynamics.

An even better exercise is to extract λ_L from the plots of λ_i versus ℓ_w/ℓ . This helps the extrapolation of λ_i to the $x = \infty$ limit, thereby eliminating any corrections, if present, for small x via judicial identification of the trends of a data set. These plots are shown in Fig. 5(c). From Fig. 5(b) it was already clear that the corrections are weak in this case, and so, in Fig. 5(c) also we observe flat behavior of the relevant region and obtain the same values of λ_L . A similar procedure is followed in the nonconserved case as well. The above-mentioned flat behavior in the intermediate regime also confirms that there exists a power-law relationship between $C_{ag}(t, t_w)$ and ℓ/ℓ_w . We reemphasize that the plots of Figs. 5(b) and 5(c) are expected to convey a similar message. Nevertheless, the weak dependence of λ_i on x , if any, will be detectable in one exercise better than the other. The exercises in these figures

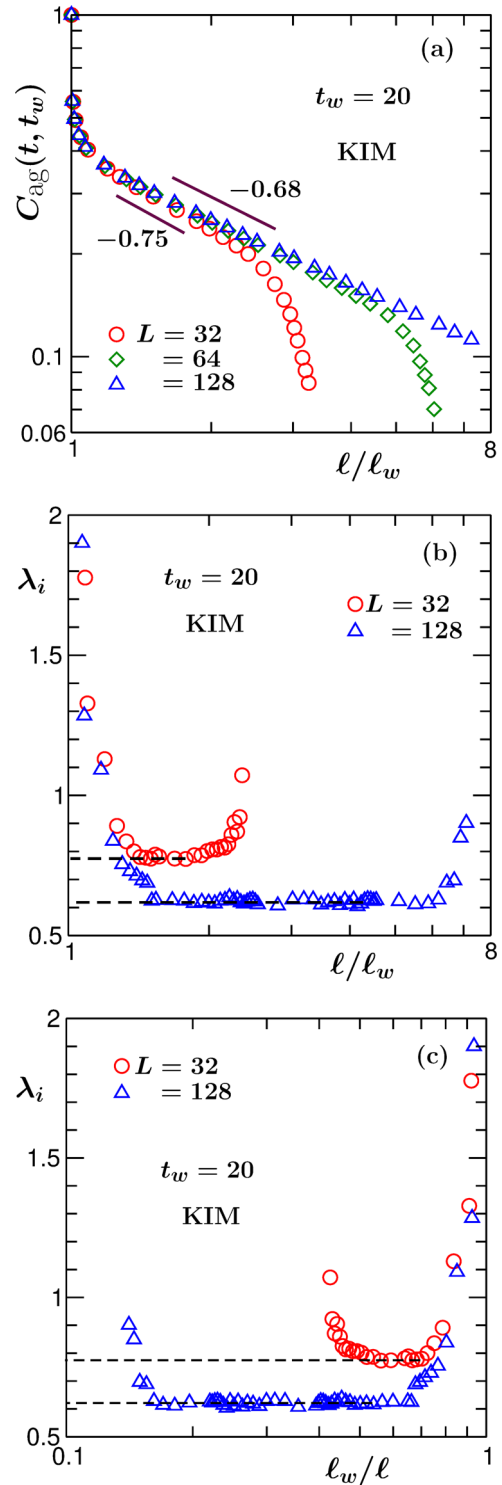


FIG. 5. (a) Log-log plots of $C_{ag}(t, t_w)$ vs ℓ/ℓ_w for $t_w = 20$ and different values of the linear dimension of the simulation box in $d = 3$. The solid lines represent power laws. (b) Plots of the instantaneous exponents, λ_i , vs ℓ/ℓ_w , for $t_w = 20$ and two values of L in $d = 3$. (c) Same as (b), but $C_{ag}(t, t_w)$ is plotted vs ℓ_w/ℓ . The dashed horizontal lines represent the estimated values of λ_L , the L -dependent aging exponent. All results are from the conserved dynamics.

suggest that the corrections in the values of λ_L that may appear due to such weak dependence are within small numerical errors.

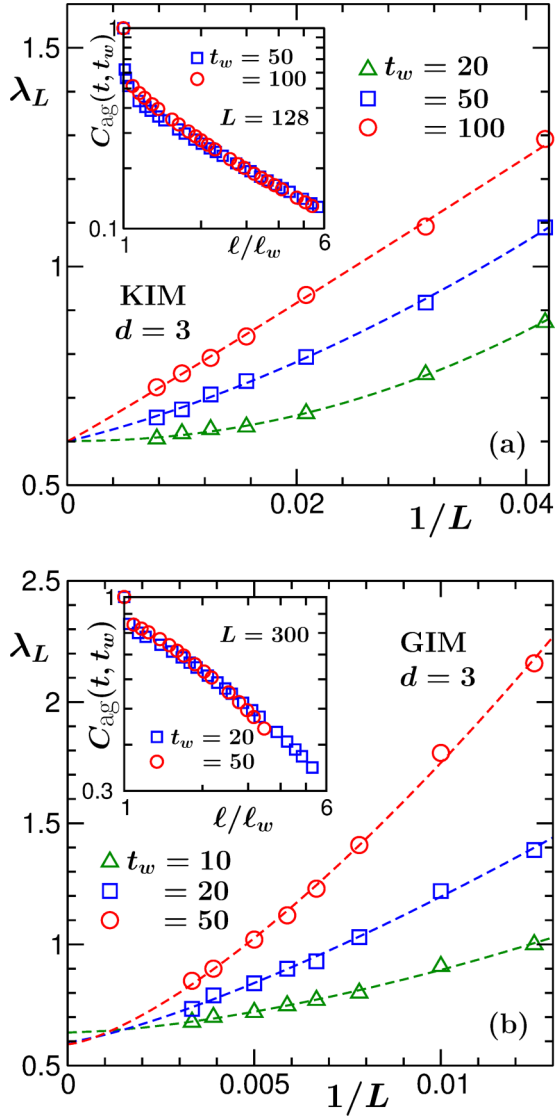


FIG. 6. (a) Plots of λ_L vs $1/L$ for the conserved order-parameter dynamics. Data from a few different values of t_w are shown. The dashed lines are power-law fits to the simulation data sets. (b) Same as (a) but for the nonconserved order parameter dynamics. All results are from $d = 3$. In both parts insets contain scaling plots of the autocorrelation function. The values of L and t_w are mentioned inside the frames.

Data for λ_L , for a particular type of dynamics, when plotted versus $1/L$ for multiple values of t_w should provide a good sense of convergence [26]. The corresponding number should be the value of λ for a thermodynamically large system. This exercise has been shown in Fig. 6 for both conserved (a) and nonconserved (b) dynamics. The dashed lines there are fits to the form

$$\lambda_L = \lambda + AL^{-b}, \quad (13)$$

where A and b are constants. For both KIM and GIM, fits to each of the data sets provides λ value quite consistent with the others. In Fig. 7 we show analogous results for $d = 2$ – part(a) for KIM and part(b) for GIM. Compared to Ref. [26], these results are obtained after averaging over a larger number

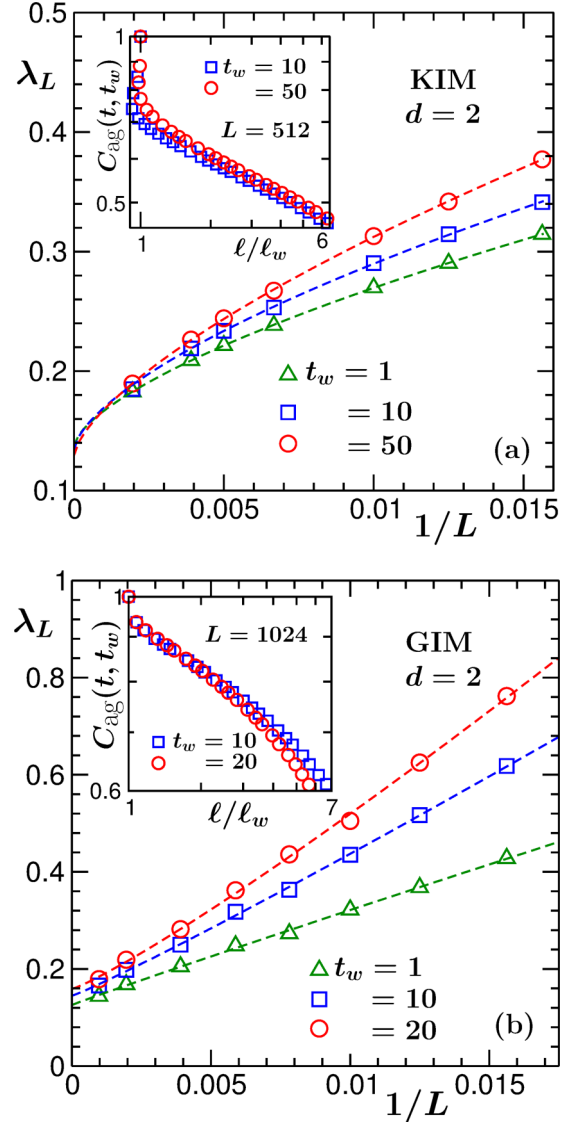


FIG. 7. Same as Fig. 6, but here the results are from $d = 2$.

of initial realizations. In the insets of Figs. 6 and 7, we show scaling plots of the autocorrelation function. Given that we have chosen the largest simulated system sizes, the collapse of data from different t_w values in each of the cases is good. The estimated values of λ are quoted in Table I, obtained after averaging over the convergences of the fittings by considering

TABLE I. List of values of λ for the nearest-neighbor Ising model. Here “Correlated” and “Uncorrelated” imply results for quenches from $T_s = T_c$ and $T_s = \infty$, respectively. For the GIM, we have quoted the theoretical predictions [8,17,21] inside the parentheses. For the values of the lower bounds [9], please see Table II.

Model	$d = 2$		$d = 3$	
	Correlated	Uncorrelated	Correlated	Uncorrelated
KIM	0.13 ± 0.02	3.6 ± 0.2	0.64 ± 0.05	7.5 ± 0.4
GIM	0.14 ± 0.02 (0.125)	1.32 ± 0.04 (1.29)	0.57 ± 0.07 (0.5)	1.69 ± 0.04 (1.67)

TABLE II. List of β values for the nearest-neighbor Ising model. Validity of YRD bound can be checked by putting these numbers in Eq. (7) and comparing the outcome with the results quoted in Table I. While preparing this table, η in $d = 3$ has been set to zero (see discussion in the context of Fig. 3). For the sake of convenience, we have put the values of the bounds [9] inside the parentheses.

Model	$d = 2$		$d = 3$	
	Correlated	Uncorrelated	Correlated	Uncorrelated
KIM	-1.75 (0.125)	4 (3)	-2 (0.5)	4 (3.5)
GIM	-1.75 (0.125)	0 (1)	-2 (0.5)	0 (1.5)

different numbers of data points for each t_w , along with those for uncorrelated initial configurations [8,14,18]. All numbers in this table are from simulation studies. For the comparison of these numbers with the YRD bound, in Table II we have quoted the values of β for 50 : 50 starting composition of up and down spins (see caption for more details) [26,32]. For the uncorrelated case it is clear that the structures are different for the conserved and nonconserved cases. For the correlated initial configurations, even though the β values for the two types of dynamics appear the same the overall structures are different, as expected [1] (see Fig. 3).

For the sake of completeness, in Table III we list the values of the persistence exponent [5,23–25] θ for the different universality classes in $d = 2$ and 3. Due to technical difficulty of estimation in the conserved case, for this quantity we quote only the values for the nonconserved dynamics. This table contains the values of fractal dimensionality (d_f) of the scaling structures formed by the persistent spins as well [25,51,52]. From the values of the quantities presented in Table III, it is again clear that the universalities for correlated and uncorrelated initial configurations are different. For the domain growth, of course, as previously mentioned, the value of n does not differ between the correlated and uncorrelated initial configurations [17,21,50].

IV. CONCLUSION

Universality in kinetics of phase transition [1] is less robust compared to that in equilibrium critical phenomena [27,34,45]. In kinetics, the classes are decided [1] by transport mechanism, space dimension, order-parameter symmetry, and its conservation, etc. In each of these cases there can be further division into universality classes [17,23–26] based on the range of spatial correlation in the initial configurations. In this paper we have examined the influence of long-range

TABLE III. List of values of the persistence exponent θ and related fractal dimension (d_f) for the nonconserved Ising model [25].

Exponent	$d = 2$		$d = 3$	
	Correlated	Uncorrelated	Correlated	Uncorrelated
θ	0.035	0.225	0.105	0.180
d_f	1.92	1.53	2.77	2.65

correlation on the decay of order-parameter autocorrelation function, a key quantity for the study of aging phenomena [6,7] in out-of-equilibrium systems, by quenching the nearest-neighbor Ising model [27,45] from the critical point to the ordered region. We have investigated both conserved [1] and nonconserved [1] order-parameter dynamics.

In the nonconserved case our study mimics coarsening in a uniaxial ferromagnet. On the other hand, the conserved dynamics is related to the kinetics of phase separation in solid binary mixtures. Despite difficulty due to multiple sources of finite-size effects, we have estimated the exponents for the power-law fall of the autocorrelation function rather accurately. We observe that in both the cases the decays are significantly slower than those for the quenches from perfectly random initial configurations [6–8,14,18].

Even though for quenches with $\xi = 0$ the values of λ differ significantly in the two cases, for quenches from the critical point, i.e., for $\xi = \infty$, the exponents are practically the same. This is irrespective of the space dimension. For the magnetic case there exists analytical prediction [17], and the numbers obtained from our simulations are in reasonable agreement with the former. The source of deviations that exists may have its origin in the estimation error for T_c^L as well as in the statistical error in nonequilibrium simulations. The discrepancy in $d = 3$ may still be real given that KIM and GIM numbers from our analysis are quite close to each other.

In the literature of aging phenomena there exist lower bounds [7,9] for the values of λ . Our results for both types of dynamics are consistent with one of these bounds. This we have checked, via the analysis of structure, a property that is embedded in the construction of the bound.

This work, combined with a few others [14,17,18,23–26], provides near-complete information on the universality in coarsening dynamics in the Ising model involving “realistic” space dimensions, the conservation property of the order parameter, and spatial correlations in the initial configurations. Analogous studies in other systems should be carried out by employing the methods used here to obtain a more complete understanding, e.g., of the influences of hydrodynamics on relaxation in out-of-equilibrium systems with long-range initial correlations.

[1] A. J. Bray, *Adv. Phys.* **51**, 481 (2002).

[2] K. Binder, in *Phase Transformation of Materials*, edited by R. W. Cahn, P. Haasen, and E. J. Kramer (Wiley VCH, Weinheim, 1991), Vol. 5, p. 405.

[3] A. Onuki, *Phase Transition Dynamics* (Cambridge University Press, Cambridge, UK, 2002).

[4] R. A. L. Jones, *Soft Condensed Matter* (Oxford University Press, Oxford, UK, 2002).

[5] A. J. Bray, S. N. Majumdar, and G. Schehr, *Adv. Phys.* **62**, 225 (2013).

[6] M. Zennetti, in *Kinetics of Phase Transitions*, edited by S. Puri and V. Wardhawan (CRC Press, Boca Raton, FL, 2009).

- [7] D. S. Fisher and D. A. Huse, *Phys. Rev. B* **38**, 373 (1988).
- [8] F. Liu and G. F. Mazenko, *Phys. Rev. B* **44**, 9185 (1991).
- [9] C. Yeung, M. Rao, and R. C. Desai, *Phys. Rev. E* **53**, 3073 (1996).
- [10] M. Henkel, A. Picone, and M. Pleimling, *Europhys. Lett.* **68**, 191 (2004).
- [11] C. Yeung and D. Jasnow, *Phys. Rev. B* **42**, 10523 (1990).
- [12] F. Corberi, E. Lippiello, and M. Zannetti, *Phys. Rev. E* **74**, 041106 (2006).
- [13] E. Lorenz and W. Janke, *Europhys. Lett.* **77**, 10003 (2007).
- [14] J. Midya, S. Majumder, and S. K. Das, *J. Phys. Condens. Matter* **26**, 452202 (2014).
- [15] S. Paul and S. K. Das, *Phys. Rev. E* **96**, 012105 (2017).
- [16] S. Roy, A. Bera, S. Majumder, and S. K. Das, *Soft Matter* **15**, 4743 (2019).
- [17] A. J. Bray, K. Humayun, and T. J. Newman, *Phys. Rev. B* **43**, 3699 (1991).
- [18] J. Midya, S. Majumder, and S. K. Das, *Phys. Rev. E* **92**, 022124 (2015).
- [19] E. Lippiello, A. Mukherjee, S. Puri, and M. Zannetti, *Europhys. Lett.* **90**, 46006 (2010).
- [20] F. Corberi and R. Villavicencio-Sanchez, *Phys. Rev. E* **93**, 052105 (2016).
- [21] K. Humayun and A. J. Bray, *J. Phys. A: Math. Gen.* **24**, 1915 (1991).
- [22] S. B. Dutta, *J. Phys. A: Math. Theor.* **41**, 395002 (2008).
- [23] T. Blanchard, L. F. Cugliandolo, and M. Picco, *J. Stat. Mech.: Theor. Expt.* (2014) P12021.
- [24] S. Chakraborty and S. K. Das, *Eur. Phys. J. B* **88**, 160 (2015).
- [25] S. Chakraborty and S. K. Das, *Phys. Rev. E* **93**, 032139 (2016).
- [26] S. K. Das, K. Das, N. Vadakkayil, S. Chakraborty, and S. Paul, *J. Phys. Condens. Matter* **32**, 184005 (2020).
- [27] M. E. Fisher, *Rep. Prog. Phys.* **30**, 615 (1967).
- [28] J. F. Marko and G. T. Barkema, *Phys. Rev. E* **52**, 2522 (1995).
- [29] M. E. Fisher and M. N. Barber, *Phys. Rev. Lett.* **28**, 1516 (1972).
- [30] D. W. Heermann, L. Yixue, and K. Binder, *Physica A* **230**, 132 (1996).
- [31] S. Majumder and S. K. Das, *Phys. Rev. E* **84**, 021110 (2011).
- [32] C. Yeung, *Phys. Rev. Lett.* **61**, 1135 (1988).
- [33] K. Binder and D. W. Heermann, *Monte Carlo Simulations in Statistical Physics* (Springer, Switzerland, 2019).
- [34] D. P. Landau and K. Binder, *A Guide to Monte Carlo Simulations in Statistical Physics* (Cambridge University Press, Cambridge, UK, 2009).
- [35] D. Frenkel and B. Smit, *Understanding Molecular Simulations: From Algorithms to Applications* (Academic Press, San Diego, CA, 2002).
- [36] K. Kawasaki, in *Phase Transition and Critical Phenomena*, edited by C. Domb and M. S. Green (Academic, New York, 1972), Vol. 2, p. 443.
- [37] R. J. Glauber, *J. Math. Phys.* **4**, 294 (1963).
- [38] U. Wolff, *Phys. Rev. Lett.* **62**, 361 (1989).
- [39] P. C. Hohenberg and B. I. Halperin, *Rev. Mod. Phys.* **49**, 435 (1977).
- [40] S. Roy and S. K. Das, *Europhys. Lett.* **94**, 36001 (2011).
- [41] S. K. Das, S. Roy, S. Majumder, and S. Ahmad, *Europhys. Lett.* **97**, 66006 (2012).
- [42] E. Luijten, M. E. Fisher, and A. Z. Panagiotopoulos, *Phys. Rev. Lett.* **88**, 185701 (2002).
- [43] S. K. Das, Y. C. Kim, and M. E. Fisher, *Phys. Rev. Lett.* **107**, 215701 (2011).
- [44] J. Midya and S. K. Das, *J. Chem. Phys.* **146**, 044503 (2017).
- [45] M. Plischke and B. Bergersen, *Equilibrium Statistical Physics* (World Scientific, London, 2005).
- [46] S. M. Allen and J. W. Cahn, *Acta Metall.* **27**, 1085 (1979).
- [47] I. M. Lifshitz and V. V. Slyozov, *J. Phys. Chem. Solids* **19**, 35 (1961).
- [48] D. A. Huse, *Phys. Rev. B* **34**, 7845 (1986).
- [49] J. G. Amar, F. E. Sullivan, and R. D. Mountain, *Phys. Rev. B* **37**, 196 (1988).
- [50] N. Vadakkayil, K. Das, S. Paul, and S. K. Das (unpublished).
- [51] G. Manoj and P. Ray, *J. Phys. A* **33**, 5489 (2000).
- [52] S. Jain and H. Flynn, *J. Phys. A* **33**, 8383 (2000).